Gas Sorption and Barrier Properties of Polymeric Membranes from Molecular Dynamics and Monte Carlo Simulations

Ioana Cozmuta,[†,‡] Mario Blanco,[‡] and William A. Goddard III*[,‡]

ELORET Corporation, NASA Ames Research Center, Moffett Field, California 94035, and Material and Process Simulation Center, California Institute of Technology, Mail Code BI 139-74, Pasadena, California 91125

Received: May 14, 2006; In Final Form: November 3, 2006

It is important for many industrial processes to design new materials with improved selective permeability properties. Besides diffusion, the molecule's solubility contributes largely to the overall permeation process. This study presents a method to calculate solubility coefficients of gases such as O_2, H_2O (vapor), N_2, and CO_2 in polymeric matrices from simulation methods (Molecular Dynamics and Monte Carlo) using first principle predictions. The generation and equilibration (annealing) of five polymer models (polypropylene, polyvinyl alcohol, polyvinyl dichloride, polyvinyl chloride-trifluoroethylene, and polyethylene terephtalate) are extensively described. For each polymer, the average density and Hansen solubilities over a set of ten samples compare well with experimental data. For polyethylene terephtalate, the average properties between a small ($n = 10$) and a large ($n = 100$) set are compared. Boltzmann averages and probability density distributions of binding and strain energies indicate that the smaller set is biased in sampling configurations with higher energies. However, the sample with the lowest cohesive energy density from the smaller set is representative of the average of the larger set. Density-wise, low molecular weight polymers tend to have on average lower densities. Infinite molecular weight samples do however provide a very good representation of the experimental density. Solubility constants calculated with two ensembles (grand canonical and Henry's constant) are equivalent within 20%. For each polymer sample, the solubility constant is then calculated using the faster (10×) Henry's constant ensemble (HCE) from 150 ps of NPT dynamics of the polymer matrix. The influence of various factors (bad contact fraction, number of iterations) on the accuracy of Henry's constant is discussed. To validate the calculations against experimental results, the solubilities of nitrogen and carbon dioxide in polypropylene are examined over a range of temperatures between 250 and 650 K. The magnitudes of the calculated solubilities agree well with experimental results, and the trends with temperature are predicted correctly. The HCE method is used to predict the solubility constants at 298 K of water vapor and oxygen. The water vapor solubilities follow more closely the experimental trend of permeabilities, both ranging over 4 orders of magnitude. For oxygen, the calculated values do not follow entirely the experimental trend of permeabilities, most probably because at this temperature some of the polymers are in the glassy regime and thus are diffusion dominated. Our study also concludes large confidence limits are associated with the calculated Henry's constants. By investigating several factors (terminal ends of the polymer chains, void distribution, etc.), we conclude that the large confidence limits are intimately related to the polymer's conformational changes caused by thermal fluctuations and have to be regarded—at least at microscale—as a characteristic of each polymer and the nature of its interaction with the solute. Reducing the mobility of the polymer matrix as well as controlling the distribution of the free (occupiable) volume would act as mechanisms toward lowering both the gas solubility and the diffusion coefficients.

1. Introduction

The adsorption of small molecules in polymeric matrices is of great scientific interest for applications ranging from catalysis to separation technology, to development of new polymeric membranes with improved barrier properties. Of particular interest are polymer materials that serve as barriers to gases, vapors, and liquids, especially those that reduce permeability to oxygen gas and water vapor. The large variety of existing polymeric membranes may exhibit barrier properties that are very different with respect to gas and water vapor.[1] Thus, the question that most naturally occurs is what makes a polymeric membrane a good barrier?

To quantify and characterize the barrier properties of a polymer film or membrane, the most frequently measured and reported quantity is the permeability P, by definition written as

$$P = \frac{(\text{quantity of permeant}) \times (\text{film thickness})}{(\text{area}) \times (\text{time}) \times (\text{pressure drop across membrane})} \quad (1)$$

This definition, mostly employed by experimentalists, corresponds to a gas permeant at two different pressures on opposite sides of "a 1-mm-thick" membrane.[2] A molecular representation corresponding to this definition would result in an extremely large system for which permeability calculations are computationally expensive, if feasible at all.

Alternatively, the permeability of a polymeric membrane is defined as the product between the diffusion coefficient, D, and the solubility coefficient, S, of the penetrant in the bulk polymer:

$$P = DS \quad (2)$$

The corresponding SI units are $cm^2\ s^{-1}$ for D and cm^3 of gas at STP per volume of polymer (cm^3) and gas pressure (Pa) for S.

* Corresponding author. Material and Process Simulation Center, California Institute of Technology, Mail Code BI 139-74, Pasadena, CA 91125. Telephone: (626) 395-2731. Fax: (626) 585-0918. E-mail: wag@wag.caltech.edu.

† ELORET Corportation.

‡ Material and Process Simulation Center.

10.1021/jp062942h CCC: $37.00
Published on Web 03/08/2007

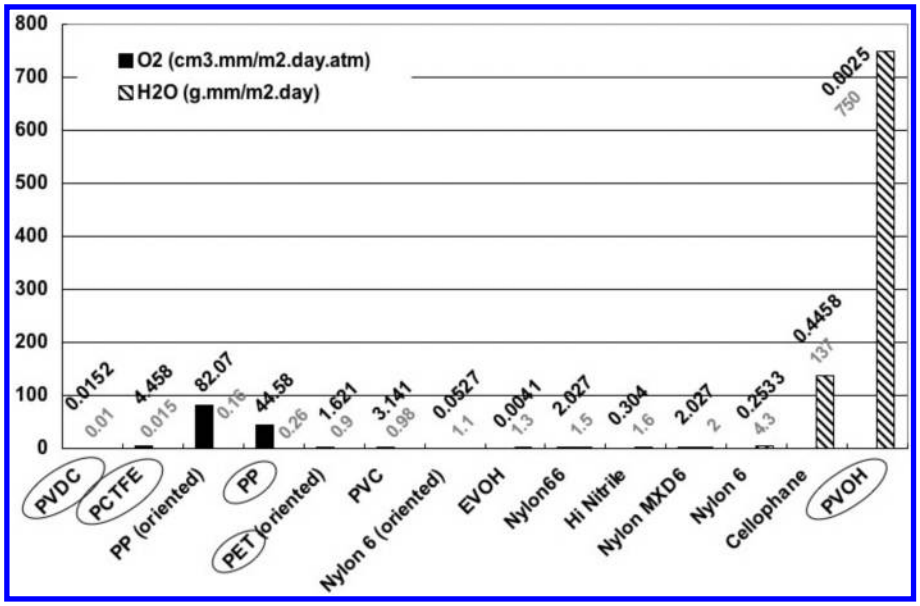

Figure 1. Experimental permeabilities for water vapor and oxygen for various polymeric membranes.[1] Selected membranes exhibiting high, low, and average barrier properties for oxygen and water vapor are modeled in the present study.

Atomistic studies of gas permeation for two models of glassy polyimide (a bulk model of the amorphous phase and a model of an actual membrane) indicate that, despite the density oscillations at the interface exhibited by the membrane model, values of the diffusion and solubility coefficients determined for the bulk model are similar to those calculated for the membrane model.[3] Thus, for molecular simulations, the permeability may be determined by separately calculating the diffusion (D) and solubility (S) coefficients for the bulk polymer under periodic boundary conditions without explicitly considering the membrane thickness.

It is known[4−6] that the diffusion coefficient and the solubility of a gas depend on various parameters characterizing the polymeric membrane (chemical structure and morphology), on the physical interactions between the penetrant and barrier material (hydrogen bonds, polar group interactions), and on environmental parameters (temperature, pressure, relative humidity). However, the key scientific interest is to study how the permeability of a certain membrane is related to its structural characteristics and to the solute−polymer interactions.

From molecular dynamics (MD) simulations of solute molecules diffusing through a bulk polymer, various parameters are obtained (especially a time scale) for Monte Carlo (MC) simulations of the diffusion coefficient at long times (∼nanoseconds). This method is described in detail elsewhere.[7] To calculate solubility properties of polymeric membranes, a combined MD and MC methodology is described here. To estimate permeabilities, the diffusion and solubility coefficients are combined via eq 2 and could further be compared to experimental data.

After a brief introduction, Section 2 describes the methods employed to generate and refine atomistic structures of various amorphous polymers. Section 3 briefly describes two statistical ensembles (Grand Canonical (GC) and Henry's constant) used in computer simulations to estimate Henry's constant and shows their equivalence. Henry's constant ensemble is then selected to calculate Henry's constant of various solutes from MD trajectories of the polymer matrix. The precision of the method with respect to various parameters in the numerical calculations is discussed. Our calculations are validated by comparing the temperature dependence (250−650 K) of nitrogen and carbon dioxide solubilities in polypropylene against other studies (Section 4.1). Section 4.2 reports solubilities of oxygen and water vapors in the five selected polymeric systems as calculated in the present study. The influence of several simulation parameters and polymer characteristics on the calculated Henry's constants is discussed (Section 4). Although in the present study solubility properties are calculated mainly for oxygen and water, this method could be applied as well for a variety of other solutes.

2. Polymer Models

Figure 1 summarizes experimentally determined permeability values with respect to water vapor and oxygen for a set of 14 polymers. For both permeants, these values range over several orders of magnitude. Also, membranes that are permeable to oxygen seem to oppose less water permeation and vice versa. For example, polyvinyl alcohol (PVOH) is very good in impeding oxygen but does not block water passage; polypropylene (PP) exhibits the contrary. In contrast, polyvinylidene chloride (PVDC) is a good barrier for both oxygen and water vapor; polyethylene terephtalate (PET) has average barrier properties for these solutes.[1] For modeling purposes, five polymers out of this set are selected on the basis of being most representative: polyvinyl alcohol (PVOH), polyvinyl dichloride (PVDC), polyvinyl chloride trifluoro-ethylene (PCTFE), polypropylene (PP), and polyethylene terephtalate (PET). The chemical structures of these five polymers are shown in Figure 2.

The Cerius2[8] amorphous builder module is used to build $n = 10$ samples for each polymer with a unit cell containing four independent molecular chains (∼1000 atoms per unit cell), each with degree of polymerization (DP) = 20. For the PET sample, a DP of 5 is used[9] and, independently, to test statistical properties of the constructed polymer samples, an additional set of $n = 100$ samples is built.

Details such as the rotational isomeric state (RIS) tables and quantum determined charges, related to the generation of the five polymer samples selected for the present study, are given in the Supporting Information.

The RIS table required as input for the amorphous builder module contains information on the conditional probability of key dihedral angles in the chain. The RIS table is determined for each polymer sample by separately minimizing the energy

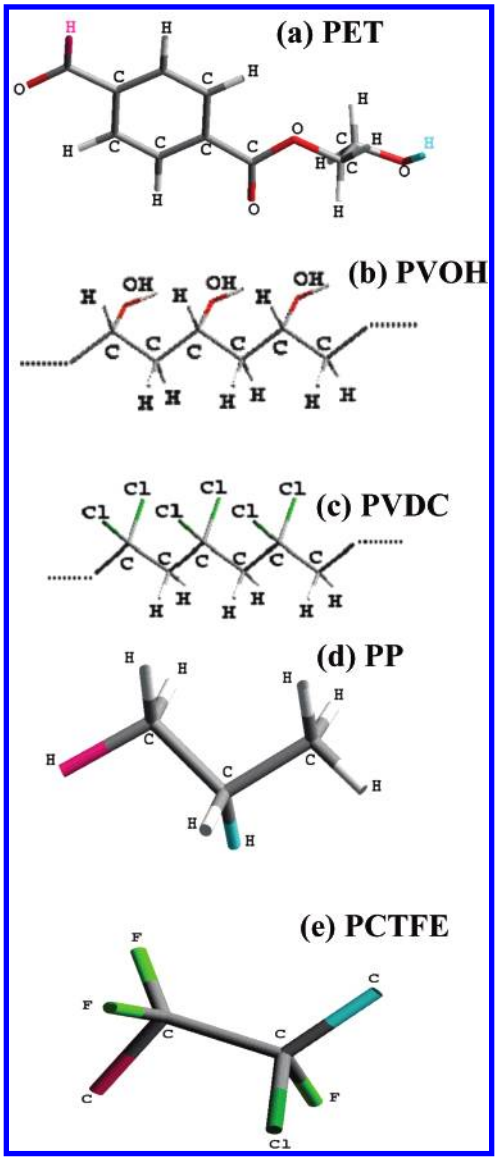

Figure 2. Chemical structures of studied polymers. For PET, PP, and PCTFE, the cis and trans ends of the monomer are colored in pink and blue, respectively, to indicate connectivity along the backbone of the polymers.

of each representative torsion, with coupling where applicable. The use of the RIS table within this building procedure ensures that polymer samples with nearly optimized geometries are produced with the proper conformational statistics. The bulk polymer samples are generated initially at low density and are modeled in an infinite periodic unit cell.

The charges on the polymers are calculated from electrostatic potential fits (ESP) to Hartree Fock quantum mechanics (QM) determined charges using the 6-31G** basis set. The atomic charges from topologically equivalent atoms are then averaged out. The QM calculations are performed for the polymers' trimers rather than for the monomers to reduce end effects. Furthermore, the charges for the terminal atoms are modified to ensure a zero net charge for the monomer.

A non-periodic (file dreidii-exp6-direct.par) and a periodic (dreidii-exp6-ewald.par) version of the Dreiding force field[10] were used for vacuum and condensed-phase calculations, respectively. These files differed only on the flags required to define the spatial extent of the nonbonding interactions. We used the Dreiding force field,[10] which is generic in that it uses general rules for the force constants and geometry parameters, based on simple hybridization considerations rather than individual parameters adjusted for each particular combination of atoms involved in the bond, angle, or torsion terms. Thus, all bond distances are derived from atomic radii, and there is only one force constant each for bonds, angles, and inversions and only six different values for torsional barriers. Combination rules are used to describe bonding and nonbonding parameters. The accuracy of Dreiding was tested against the X-ray structures for 76 organic compounds with excellent geometric parameters and conformational energies. Dreiding allows some choices in the descriptions. Thus, we used the exponential-six form for the van der Waal's parameters rather than Lennard-Jones 12-6, and we used the harmonic cosine form for angle terms rather than harmonic angle terms. For the nonbonding terms, we used no cutoffs for finite systems but Ewald optimized parameters for periodic systems.

For each of the n samples generated for each polymer, the equilibrium unit cell volumes and densities are obtained by a series of compression/expansion and heating/cooling cycles (Figure 3) according to the procedure described below.

1. The polymer sample is built in a cubic cell with a target density of 40% of the expected density, ρ_{exp} (usually chosen as the experimental value) using the RIS technique described above.

2. The structure is energy minimized holding the unit cell parameters fixed.

3. The system is compressed in four steps (0.6, 0.8, 1.0, $1.2\rho_{exp}$) to achieve a final density of $1.2\rho_{exp}$.

4. At each density, the structure is again energy minimized for 500 steps followed by 0.5 ps of NVT MD at 500 K.

5. The system is allowed to relax (expand) to a final density ρ_{exp} in four steps (1.15, 1.1, 1.05, $1.0\rho_{exp}$).

6. At each density, the structure is energy minimized for 500 steps and followed by 0.5 ps of NVT MD at 500 K.

7. The final structure resulting from step 6 is energy minimized for 500 steps and equilibrated using NPT MD for 10 ps at 298 K. The density of this final relaxed state will be close to ρ_{exp}.

At the end of the anneal dynamics cycle, several physical and chemical properties (density, solubility parameters, end-to-end distance, and radius of gyration) are calculated as averages over the number n of generated samples and reported in Table 1. Reported standard deviations correspond to the 95% confidence limit (2σ standard deviations on each side of the average). The cohesive energy density (CED) is also calculated during this cycle as the difference between the total energy of the bulk system (all terms in the energy expression) and the sum of the gas-phase energies for each of the four polymer strands composing the unit cell divided by the volume of the unit cell. The Hildebrand solubility parameters are calculated using the standard definition.[11] The last column in Table 1 represents the binding energy (E_b) per monomer averaged over the 10 ps NPT dynamics during the final step of the annealing procedure (step 7). The above procedure to generate polymeric samples will be further referred to as the CED procedure, and it is described elsewhere in more detail.[12]

To determine whether the sample set of $n = 10$ is statistically adequate, the CED procedure is repeated to generate an additional set of $n = 100$ PET samples. Four types of energies are calculated and compared for the two sets: (i) the CED per monomer, CED (cal/cc), dividing the CED values (Table 1) by the number of monomers; (ii) the energy per monomer, E_b (kcal/mol), multiplying the CED values with the volumes of each sample and dividing it by the number of monomers; (iii) the

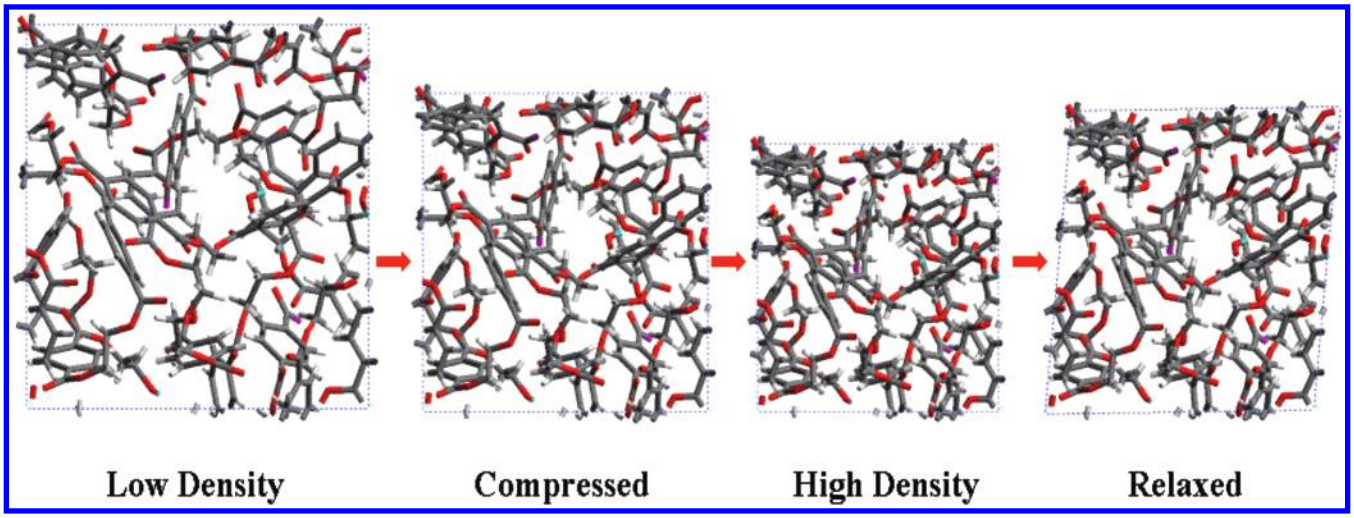

Figure 3. Anneal dynamics protocol schematized for the PET sample. The target density is the experimental density for amorphous PET, $\rho_{exp} = 1.3$ g/cm^3. The low-density state corresponds to $0.4\rho_{exp}$, the compressed state to $0.8\rho_{exp}$, and the high-density state to $1.2\rho_{exp}$. The final relaxed state targets a density close to the experimental value.

TABLE 1: Summary of Information from the Anneal Dynamics Cycle[a]

polymer (n)	no. of monomer polymers per unit cell	cohesive energy density (cal/cc)	solubility parameter (cal/cc)$^{1/2}$ calculated	solubility parameter (cal/cc)$^{1/2}$ exptl	volume (Å^3/UC)	$R_{end-end}$ (Å)	R_g (Å)	E_b (kcal/mol)
PET (10)	20	(−142.62 ± 10.71)	(11.93 ± 0.45)	[9.7−10.7]	(5076.2 ± 92.3)	(14.9 ± 0.8)	(7.04 ± 0.39)	(−21.8 ± 2.3)
PET(100)	20	(−51.49 ± 11.40)	(12.3 ± 0.46)	[9.7−10.7]	(5028.1 ± 124.0)	(14.9 ± 1.9)	(7.02 ± 0.36)	(−2.9 ± 0.7)
PVOH (10)	80	(−62.75 ± 16.38)	(16.20 ± 0.51)	[12.7−14.2]	(4856.8 ± 89.1)	(25.2 ± 3.5)	(9.52 ± 0.61)	(−3.4 ± 0.3)
PVDC (10)	80	(−71.47 ± 10.07)	(8.44 ± 0.59)	[9.3−10.8]	(8558.9 ± 293.1)	(13.8 ± 2.9)	(7.25 ± 0.56)	(−2.1 ± 0.2)
PCTFE (10)	80	(−46.14 ± 5.47)	(6.78 ± 0.40)	[7.2−7.9]	(8658.6 ± 334.9)	(17.7 ± 2.5)	(7.91 ± 0.48)	(−3.3 ± 0.3)
PP (10)	80	(−48.00 ± 5.04)	(6.91 ± 0.36)	[7.7−9.4]	(6896.4 ± 188.7)	(14.3 ± 2.3)	(6.96 ± 0.37)	(−107.8 ± 0.2)

[a] The experimental range for the solubility parameter[13,28] is listed in this table. For PET, two sets of samples ($n = 10$ and 100) are generated using the CED procedure. Experimental and calculated (present study) densities are listed in Table 3.

strain energy density per monomer, E_{sd} (cal/cc), calculating the total single point energy of each energy minimized sample and dividing the value by the unit cell volume and the number of monomers; (iv) the strain energy per monomer, E_s (kcal/mol), calculating the total single point energy of each energy minimized sample and dividing the value by the number of monomers.

The probability distributions of these energies for the $n = 10$ and 100 sets are shown in Figure 4a−d. Table 2 summarizes the normal average with the corresponding standard deviation and the Boltzmann averages (indicated by $<>_B$) calculated from

$$\langle E \rangle = \frac{\sum_j E_j \exp\left(-\frac{E_j}{k_B T}\right)}{\sum_j \exp\left(-\frac{E_j}{k_B T}\right)} \quad (3)$$

The normal averages in Table 2 indicate that, within uncertainties, the binding and mechanical energies are similar for the $n = 10$ and 100 sets. When calculating Boltzmann averages, larger emphasis is given to states with lower energy. Comparing the average values of the CED and binding energy for the two sets clearly indicates that sampling with a larger set ($n = 100$) leads to a larger number of configurations with lower energies. This is consistent with the fact that strain energy densities are larger for the samples in the smaller ($n = 10$) set. The total strain per unit cell is relatively the same for the two sample sets. This is expected because the CED procedure aims to generate structures that in their final state will be relaxed and will have densities close to ρ_{exp}. Correlating these averages with their probability distributions (Figure 4) clearly shows that by generating a smaller set of samples ($n = 10$ vs 100) the sampling is biased toward configurations with higher energies (Figure 4a,b). Both the strain energy densities, E_{sd} (Figure 4c), and the binding energies, E_b (Figure 4b), for the smaller set are biased toward larger values, indicating that the larger strain energy densities in the smaller set are responsible for the higher energy generated configurations. Despite the fact that the smaller set is not representative as a whole for the larger set, the probability distributions of the CED and binding energies (Figure 4a,b) provide a way for sample selection. The sample with the lowest CED and binding energies from the smaller set ($n = 10$) will be representative of the average of the larger set ($n = 100$). For our permeability study, this is thus the criterion we used to select a representative sample out of the generated small ($n = 10$) sets for PET, PP, PVDC, and PVOH. This sample also has, within the set, the density closest to the experimental density of the polymers (Table 3).

For the selected samples, additional 150 ps of NPT dynamics (using the Nose−Hoover thermostat and the Parrinello−Rahman barostat) at 298 K and 1 atm $= 1.0132 \times 10^{-4}$ GPa is run. The equilibrated part (last 100 ps) of the NPT−MD generated trajectories is then used for solubility calculations.

Table 3 shows the experimental densities reported for the amorphous polymers, ρ_{exp},[13] the annealing densities (averaged for all n samples from the dynamics at step 7 of the CED procedure), ρ_{anneal}, and the minimized density (from all n samples), ρ_{min}. For comparison, the densities corresponding to the lowest cohesive energy density, ρ_{CED}, and the average density from the 150 ps NPT dynamics, ρ_{NPT}, for the selected sample from the n cases are also indicated.

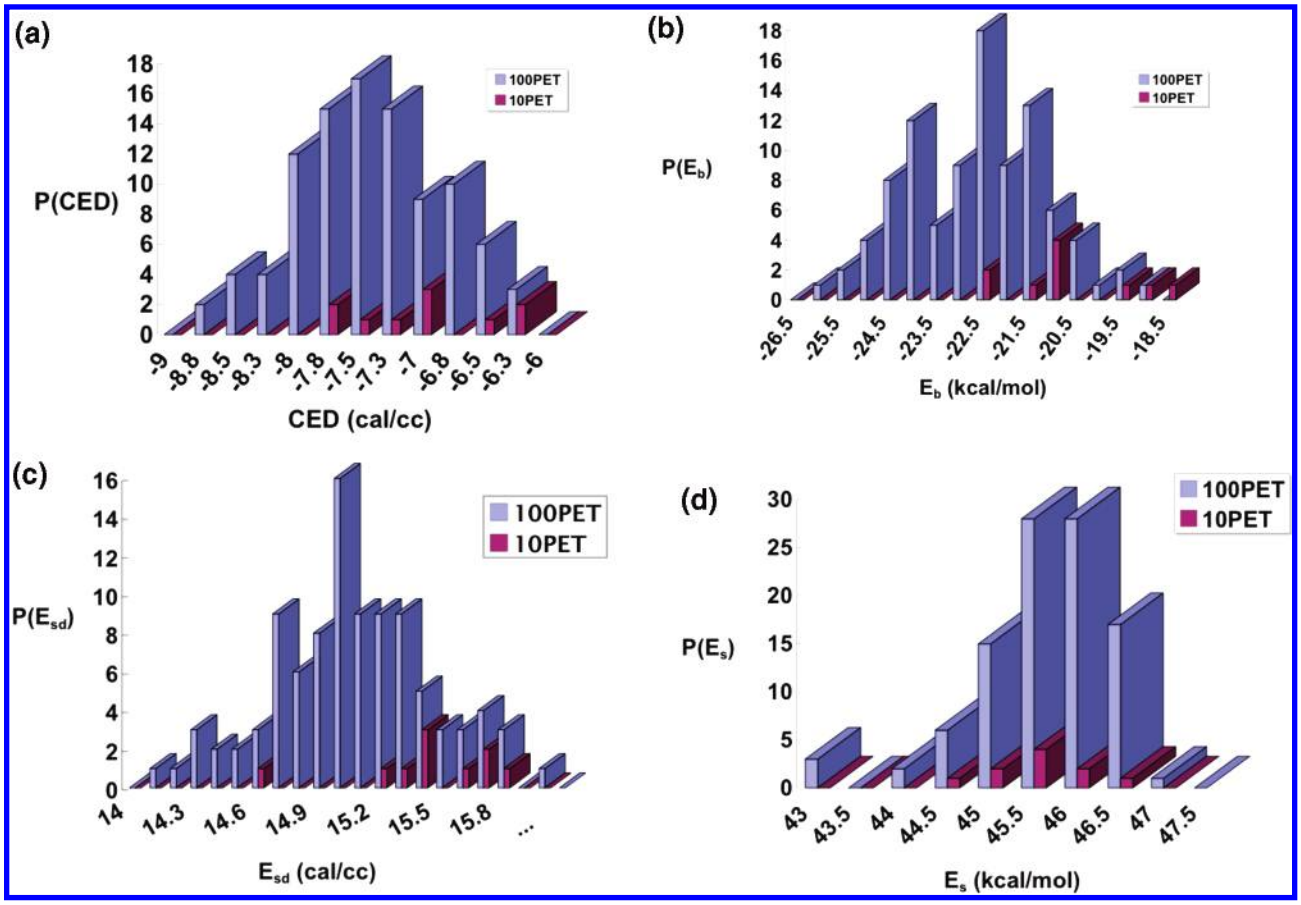

Figure 4. Probability distributions of (a) cohesive energy density, (b) cohesive energy, (c) strain energy density, and (d) strain energy per monomer of the PET polymer sample from two ($n = 10$ and 100) sets. These distributions indicate that the samples generated in the smaller set are biased toward configurations with higher energies (a, b) due to the larger existing strain densities (c) in the unit cells.

TABLE 2: Normal and Boltzmann Averages ($<>_B$) of the Energy Values for the $n = 10$ and $n = 100$ Sets of PET Samples[a]

n (PET)	CED cal/cc		E_b kcal/mol		E_{sd} cal/cc		E_s kcal/mol	
10	(-7.1 ± 0.5)	$<-7.5>_B$	(-20.9 ± 1.3)	$<-22.4>_B$	(15.4 ± 0.3)	$<15.5>_B$	(45.2 ± 0.5)	$<44.8>_B$
100	(-7.6 ± 0.6)	$<-8.1>_B$	(-22.9 ± 1.4)	$<-25.3>_B$	(15.0 ± 0.4)	$<14.8>_B$	(45.4 ± 0.7)	$<44.6>_B$

[a] Comparison between Boltzmann averages is more meaningful. The smaller set is biased toward higher energy polymer configurations due to larger existing strains in the unit cell.

TABLE 3: Comparison of Experimental Densities, ρ_{exp},[13,15] with the Densities from Annealing, ρ_{anneal}, Additional Minimization, ρ_{min}, the Density Corresponding to the Lowest Energy CED Sample, ρ_{lCED}, and One-Sample NPT Dynamics-Average, ρ_{NPT}[a]

polymer	ρ_{exp} g/cm^3	ρ_{anneal} g/cm^3	ρ_{min} g/cm^3	ρ_{lCED} g/cm^3	ρ_{NPT} g/cm^3
PET10	1.34	1.26 ± 0.02 (6%)	1.31 ± 0.02 (2%)	1.29 (4%)	1.29 ± 0.03 (4%)
PET100	1.34	1.a27 $\pm$ 0.03 (5%)	1.32 ± 0.03 (1.5%)	1.31 (2%)	
PVOH	1.29	1.21 ± 0.02 (6%)	1.21 ± 0.03 (6%)	1.25 (3%)	1.24 ± 0.03 (4%)
PVDC	1.66	1.51 ± 0.05 (9%)	1.57 ± 0.03 (5%)	1.62 (2.5%)	1.64 ± 0.03 (1%)
PCTFE	2.1	1.79 ± 0.07 (15%)	1.89 ± 0.07 (10%)	1.90 (10%)	1.77 ± 0.05 (16%)
PP	0.86	0.81 ± 0.03 (6%)	0.82 ± 0.02 (5%)	0.86 (0%)	0.86 ± 0.03 (0%)

[a] Between brackets, the percentage deviations from experimental values are indicated. The density of the lowest energy CED sample compares well to the experimental density.

The ρ_{anneal} values are low by ~6% to 15% compared to experimental densities (ρ_{exp}) due to the dynamic fluctuations of the polymer matrix (from the NPT dynamics performed at step 7 of the CED cycle) as well as the statistical nature of the generated sample set, based on n samples. The discrepancy with experimental densities is reduced to about ~2−10% (2−5% if the PCTFE sample is not included) when additional energy minimization is performed (ρ_{min}). The best comparison with experimental densities is given by ρ_{lCED} and ρ_{NPT}. The densities of the sample with the lowest CED energy (ρ_{lCED}) are underestimating experimental densities 2−10% (2−4% if not including PCTFE). The ρ_{NPT} values, calculated as average densities over the additional NPT dynamics of the equilibrated selected (lowest CED energy) polymer samples, underestimate experimental densities by 1−16% (1−4% if not including PCTFE). Out of the set of five polymers, the poorest comparison with experimental data is obtained for PCTFE most probably because the force field does not include a good enough

description of the interaction potentials characteristic for fluoride atoms. For this reason, solubility values for PCTFE are not calculated.

One infinite molecular weight sample is generated for the PET polymer. After annealing, the density of the PET sample is 1.334 g/cm^3, in excellent agreement with the experimental data. This leads us to the conclusion that, in general, underestimated densities are to be expected when using atomistic representations, unless infinite molecular weight representations are used, as industrial grade polymers typically have DP well over 1000, much larger than the low molecular weights polymers (DP 20) modeled in this study. Infinite molecular weight polymers are however impractical to model due to the long simulation time scales one would require.

3. Methodology to Calculate Solubility Constants

Solubility represents the ability of a substance to dissolve into another. Its value expresses the maximum amount of solute that will dissolve in a given amount of solvent. For gases in polymers, the solubility S describes the concentration C of the gas inside a polymer at equilibrium with the gas at partial pressure p and is described by the dual-mode theory:[14]

$$C = k_H p + C_\infty \frac{bp}{1+bp} \tag{4}$$

This equation accounts for two distinct mechanisms of sorption: the first term corresponds to Henry's law, proportional to p; the second term represents a Langmuir-type isotherm with C_∞ being the saturation concentration of the gas and b being the ratio of gas molecules absorption/desorption rates. The dual-mode sorption model (eq 4) is derived under the assumptions that a statistical equilibrium exists between solute particles and that the properties and structure of the host matrix are unaffected by the presence of the solute. The adsorption sites are required to be permanent, independent, and isoenergetic, and it is assumed that no more than one solute molecule is able to occupy a site at one time. The above equation applies to homogeneous host matrices (the polymeric system in the present case) and describes the solubility properties of fast diffusing small molecules well.

For ideal dilute solutions (real solutions at low concentrations), the case of gases in rubbery polymers, one may ignore the Langmuir part in eq 4. For such rubbery polymers, Henry's law is obeyed up to pressures of several hundred atmospheres.[15,16] The relation between solubility and Henry's constant (expressed in standard units of Pa^{-1}) can be derived by assuming that the gas exhibits ideal gas behavior both at STP conditions (T_0 = 273.15 K, p_0 = 1 atm) and at the temperature of the measurements (i.e., V/V (STP) = T/273.15 K)

$$S = k_H \frac{T}{273.15\ \mathrm{K}} \tag{5}$$

In computer simulations, Henry's constant is usually calculated via Monte Carlo statistical mechanics methods.[17,18] There are two equivalent modalities to perform such calculations. The first requires the evaluation of the simulation-cell loading at several fixed pressures (Grand Canonical Ensemble (GCE)). Henry's constant, k_H, is then calculated as the simulation-cell loading, C, divided by the sorbate pressure, p, in the limit of zero pressure:

$$k_H = \lim_{p \to 0} \frac{C}{p} \tag{6}$$

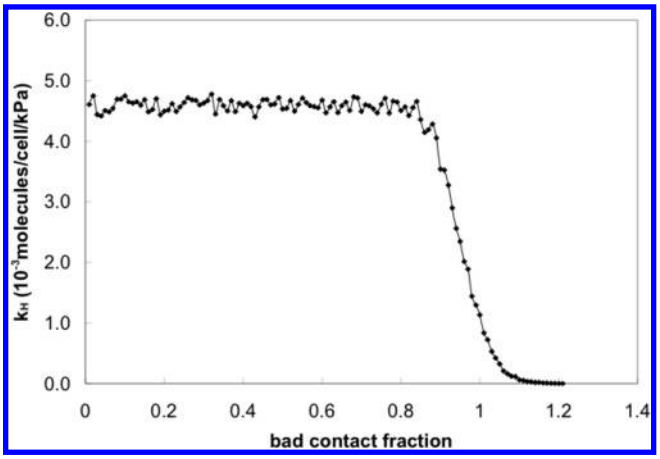

Figure 5. k_H versus the bad contact rejection factor, f. A close contact occurs when two atoms approach within a defined fraction f of the sum of their van der Waals radii. The value of $f = 0.5$ is considered in Henry's Constant Ensemble calculations.

Bezus[19] proved that k_H could be computed from configuration integrals corresponding to different positions (r) and orientations (Θ) of the solute molecule inside the cavities of the polymer matrix:

$$k_H = \frac{1}{k_B T} \int_{\mathrm{cell}} \mathrm{d}r \int \frac{\mathrm{d}\Theta}{8\pi^2} \exp^{\frac{-U(r,\Theta)}{k_B T}} \tag{7}$$

In practice, these cavities are partitioned into small cells and the energies of interaction, $U(r,\Theta)$, are calculated at the centers of these cells. It is assumed that at any point inside a given cell the corresponding contribution to the total energy of interaction is equal to the value calculated for the center of the cell. Thus, the integral in eq 7 becomes the finite sum:

$$k_H \approx \frac{V_{\mathrm{cell}}}{k_B T} \frac{1}{N} \sum_i \exp\left(\frac{-U(r_i,\Theta_i)}{k_B T}\right) \tag{8}$$

with V_{cell} being the volume of the unit cell and N being the adjustable number of steps in the simulation. The positions (r_i) and orientations (Θ_i) are chosen at random.[19] This procedure is implemented in Cerius2 under the choice of Henry's constant ensemble[8] and requires as input the model of the polymer framework and a model of the sorbate molecule of interest. The program will then generate N random positions and orientations for the sorbate molecule. For all accepted configurations, the solute−matrix and the solute−solute (images) interaction energies are calculated and added to the sum in eq 8. Henry's constant is returned at the end of the calculation in units of molecules/unit cell/kPa. Throughout this paper, we will report values of k_H in cm^3 (STP) cm^{-3} atm^{-1}, because experimental data are usually expressed in terms of volume of gas at standard temperature and pressure (STP) adsorbed in a certain volume of polymeric material at the pressure of interest, p.

Accepted configurations depend upon a bad contact rejection fraction parameter set by the user. Before performing an energy calculation, the program checks for close contacts to identify and reject such high-energy configurations (that would give negligible contributions to the sum) to save calculation time. A close contact occurs when two atoms approach within a defined fraction f of the sum of their van der Waals radii. In the present calculations, a value of 0.5 is chosen for this fraction.

Figure 5 shows the variation of the solubility coefficient (k_H) as a function of the bad contact rejection fraction f calculated

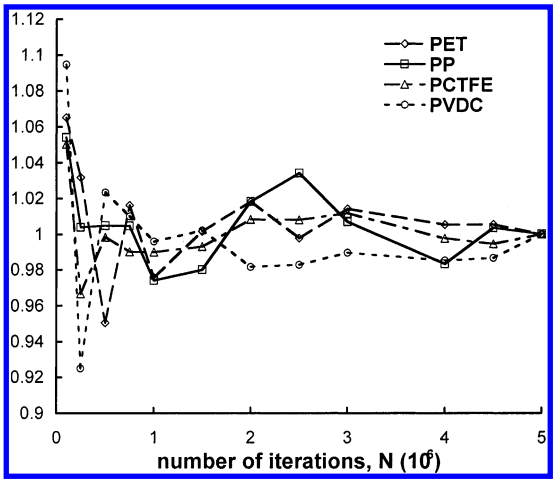

Figure 6. Calculated k_H values as a function of the number of terms, N, in the sum of eq 8. All k_H values are normalized to the converged value obtained for $N = 5 \times 10^6$ iterations. A number of iterations of $N = 1.5 \times 10^6$ provides a satisfactory convergence criteria without being computationally too expensive and is used throughout the present study.

for one frame of the PET sample. If the value of f is too large, many bad contacts will be found, the calculation will be fast but inaccurate. In contrast, if f is too small, too many high-energy configurations are accepted, slowing down the calculation without correspondingly increasing the accuracy.

Another adjustable setting in the numerical calculation of k_H is the number of iterations (N, the number of terms in the sum of eq 8). Calculations are carried out for the PET, PP, PCTFE, and PVDC polymer samples to check how the precision in the k_H determination depends on the number of iterations, N. For each N, varied from 1.5×10^5 to 5×10^6 steps, k_H is normalized by the value calculated for $N = 5 \times 10^6$. Figure 6 shows that $N = 1.5 \times 10^6$ steps is sufficient to obtain a well-converged value of k_H (within 4%) and is also convenient from the point of view of computational time (that in principle scales with N). This value, if not otherwise specified, is used throughout this paper.

Usually, Henry's constant calculations are performed on rigid frameworks (zeolites, aluminophosphates, etc.) with a microporous structure that does not change significantly during dynamics simulations. However, for polymeric systems, it is observed that the dynamics of the polymer matrix introduces important structural modifications (distribution of voids and channels, destruction of existing voids, and generation of new ones). Because the existing free volume and its distribution inside the host matrix influences both diffusion and sorption (see also Figure 9 and Figure 10), k_H is calculated as the average over a selected number of frames (every 0.5 ps) in the equilibrated part (usually 50−150 ps) of each MD trajectory. For statistical purposes, a confidence interval rather than an average value is calculated for k_H according to a two-tailed test and a 95% confidence level:

$$\bar{x} - t_{\alpha,n-1}\frac{s}{\sqrt{n}} < \mu \leq \bar{x} + t_{\alpha,n-1}\frac{s}{\sqrt{n}} \qquad (9)$$

In eq 9, $t_{\alpha,n-1}$ is the value of the standard normal variable that puts $\alpha/2\%$ in each tail of the distribution, μ is the population mean, n is the sample size, $\bar{x}$ is the sample mean, and $s/\sqrt{n}$ is the standard error for $\bar{x}$. This procedure is further referred to as the "Henry's constant ensemble" (HCE) method. To evaluate the energy expression in the HCE calculations, the Dreiding

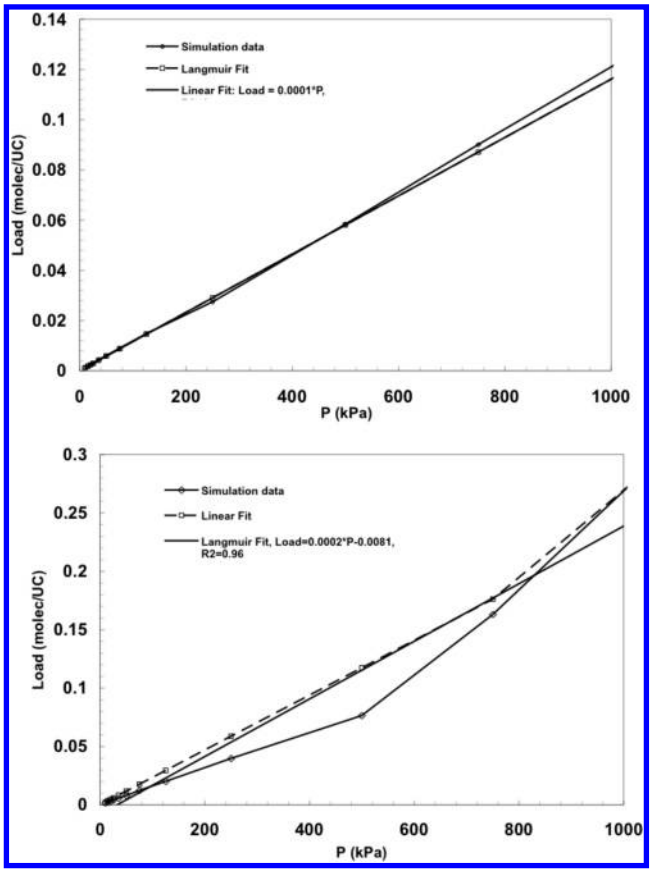

Figure 7. Concentration vs pressure calculation (grand canonical ensemble) for the PET sample with H_2O (top) and O_2 (bottom). Equation 4 is then fit through the data points (Langmuir and linear). The calculated fit parameters are $k_H = 1.16 \times 10^{-4}$, $b = 0.99$, $c_\infty = 1.74 \times 10^{-7}$ for water and $k_H = 2.35 \times 10^{-4}$, $b = 0.05$, $c_\infty = 0.05$ for oxygen. Together with the data in Table 4, this indicates that HEC and GC ensemble calculations are equivalent, with HEC providing a faster method for solubility calculations.

force field[10] is used. The procedure employs the minimum image convention to calculate the van der Waals component of the energy and the Ewald summation method for the Coulomb interactions. However, the latter can be turned off for cases when the solute molecule is not charged (e.g., oxygen, nitrogen) to save computation time. The default nonbonding cutoff is initially 8.5 Å and is automatically optimized during the calculation to ensure solution consistency.[8]

Agreement of the k_H predictions given by the Grand Canonical (eq 4) and Henry's constant (eq 8) ensembles is checked. Via the GC ensemble, the solute concentration (cell load) for oxygen and water is calculated for the PET matrix for a range of pressures between 0.01 and 10 atm (Figure 7). Equation 4 is then fit through the data points to obtain k_H in the limit of zero pressure. The calculated Langmuir parameters, b and c_∞, are both essentially zero (Table 4).

The GC ensemble fit values of k_H are compared with the results from HCE in Table 4. The k_H values calculated with the two ensembles agree within 20%. Because the experimental data do not agree better than 10%, and because HCE calculation is about 10 times faster than GC, we chose to use HCE for all our further calculations.

The precision of the k_H procedure is also tested by repeating (three times) the calculation for exactly the same configuration of each of the polymers. The results show that all the calculated values are repeatable within 5%.

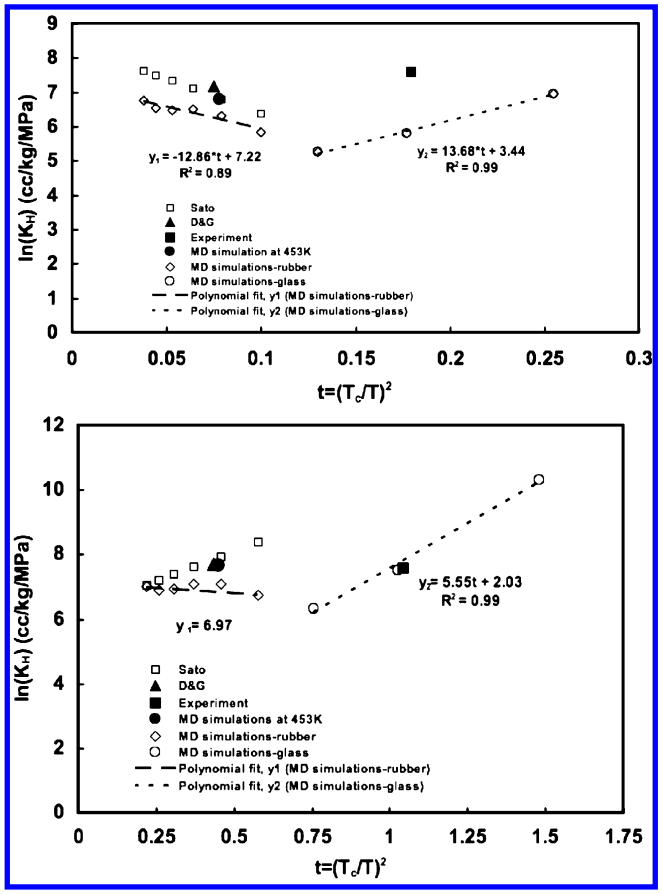

Figure 8. ln(k_H) in PP calculated in the present study (MD simulations) as a function of the reduced temperature, $t = (T_c/T)/2$, where T_c is the critical temperature of the gas, N_2 (top) and CO_2 (bottom). A first-order polynomial is fitted through the data points. Values from Table 5 are also added to the graph. The nonlinear behavior resulting from our first principles study accounts for both gas condensation, dominant at low temperatures, and solute−solvent mixing, important at higher temperatures, which the linear Sanchez−Lacombe EOS[19] does not include. For reference, a reduced temperature of $t = 0.11$ for N_2 and $t = 0.66$ for CO_2 corresponds to the glass transition temperature of the polymer matrix.

4. Results and Discussion

To validate the HCE method, the temperature dependence of nitrogen (N_2) and carbon dioxide (CO_2) solubilities in polypropylene (PP) is calculated and compared with data from other literature studies. The dynamics of the polymer matrix plays an important role in solubility calculations. Characteristic parameters of the PP polymer matrix and the temperature dependence of the polymer matrix and of the solute−polymer interaction are separately analyzed (see Supporting Information).

Using HCE, we calculated solubilities of oxygen and water vapor for the set of selected polymers (PET, PVOH, PVDC, PP). The origin of the large confidence intervals associated to the calculated Henry's constants is discussed.

4.1. Temperature Dependence of k_H. A molecular dynamics trajectory at 453.2 K is initially generated for PP. The confidence interval of k_H at this temperature for N_2 and CO_2 is estimated using HCE (Section 3). The data summarized in Table 5 compare the value from our calculation with values extracted from two other studies.

The first study by Durrill & Griskey[20] contains data on measured solubilities and diffusivities of various gases in molten or thermally softened polymers. The experimental procedure involves saturation of the polymer matrix with the gas at low pressure. As a response to the initial quick increase in pressure, the solute starts permeating the polymer. The pressure drop rate is then recorded. From the pressure versus time curves, by repeating this procedure at various pressures, the gas solubilities/k_H are calculated. The precision of the experimental data claimed by the authors is about 8%. For N_2 and CO_2 in PP, k_H values are determined at 461 K.

The second study by Sato et al.[21] reports the following linear relationship between k_H and temperature based on the Sanchez−Lacombe equation of state:

$$\text{For } N_2\text{: } \ln k_H = 8.407 - 20.39\left(\frac{T_c}{T}\right)^2$$

$$\text{For } CO_2\text{: } \ln k_H = 6.255 + 3.706\left(\frac{T_c}{T}\right)^2 \qquad (10)$$

T_c(K) is the critical temperature of the gas, and T(K) is the actual temperature of the system. The Sanchez−Lacombe EOS predicts the swelling of the polymer matrix in the presence of a gas/solute, given a certain pressure. The Sato et al. values in Table 5 are calculated from eq 10 at $T = 461$ and 453 K.

With respect to the experimental data,[20] the Sanchez−Lacombe EOS overestimates the CO_2 k_H by 17−37% and underestimates that of N_2 by 20−30%, being considered a good agreement.[21] The experimental data fall within the range predicted by the present MD simulations.

The limits of the confidence interval of k_H calculated from NPT−MD are determined by the dynamic fluctuations of the unit cell total volume (Figure B1.1, see Supporting Information) and the amount and distribution of void space (Figure B1.1, see Supporting Information).

For a more conclusive validation, the temperature dependence of k_H of N_2 and CO_2 in PP is studied for a range of temperatures between 250 and 650 K (Figure 8). This temperature range covers both the glass transition temperature (280 K) and the melting temperature (~459 K) of 100% crystalline PP. The k_H is calculated using the ensemble method described in Section 3 from every 2 ps frame along the 100 ps NPT−MD trajectories of the PP matrix determined every 50 K in the above-mentioned range.

To correlate with the data used in the Sato et al.[21] study, Stern et al.[22] proposed to use a linear expression between k_H (cc (STP)/kg MPa) and the reduced temperature $t = (T_c/T)^2$. Values of 304.1 and 126.2 K obtained from Reid et al.[23] are used for the critical temperatures, T_c, of CO_2 and of N_2, respectively. The corresponding range of reduced temperatures, t, is approximately 0.25−0.04 for N_2 and 1.5−0.21 for CO_2. For reference, the glass transition temperature of isotactic polypropylene is 373 K and corresponds to a reduced temperature of $t = 0.11$ for N_2 and $t = 0.66$ for CO_2. The k_H values determined in the present study (Figure 8) are compared with Sato's data[21] calculated from eq 10 for the rubbery regime of the polymer (temperatures between 400 and 650 K). The value determined by Durrill and Griskey[20] at 461 K is also added to Figure 8 together with our initial determination at 453 K (see also Table 5). Experimental determinations of N_2 and CO_2 solubilities in PP are mostly available for the rubbery regime where solubility is the dominant mechanism. With diffusion controlling the transport in the glassy regime, solubility determinations are usually difficult. One such experimental study[24] indicates that the solubility of N_2 and CO_2 are equal for pressures between 0.1 and 3 bar and at 298 K. The data points shown in Figure 8 by black squares agree with our calculated value for CO_2 but disagree for N_2.

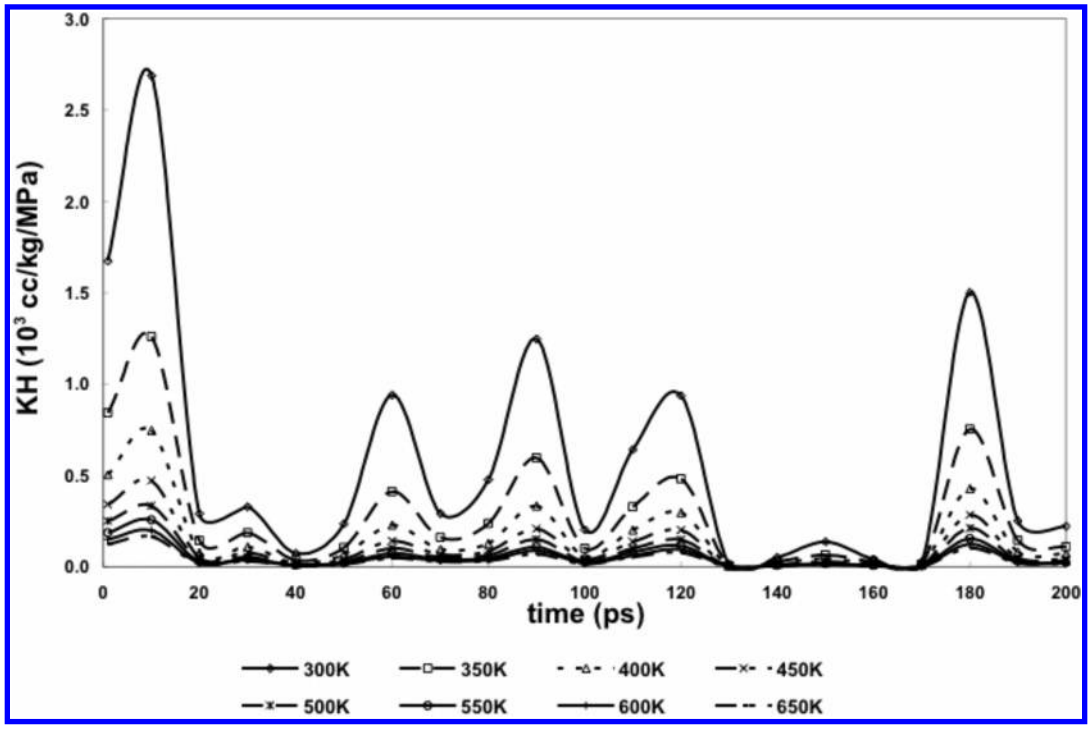

Figure 9. Time fluctuations of k_H over a dynamic trajectory for which the temperature of the polypropylene matrix is kept at 300 K and only the temperature dependence of the gas (N_2) molecule is varied from 300 to 650 K in steps of 50 K. Consistent with eq 7, k_H values scale inversely proportional with temperature and preserve identical time dependence due to unchanged $U(r,\Theta)$ values.

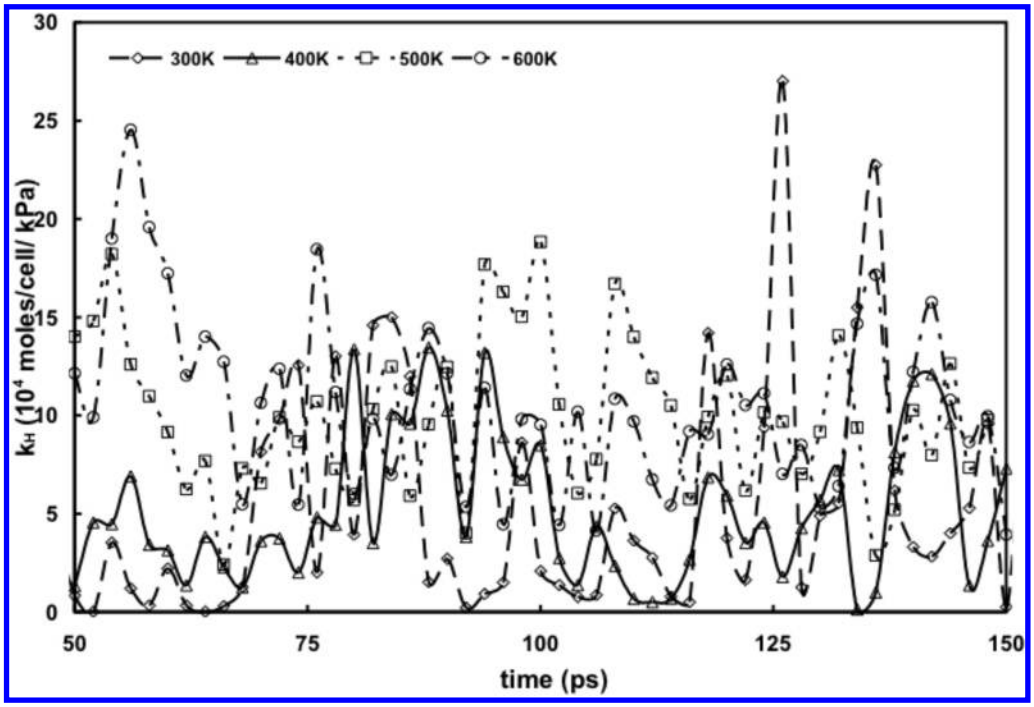

Figure 10. Time fluctuations of k_H of N_2 for four temperatures where the dynamics of the polymer (PP) matrix as function of temperature is considered. On top of the fluctuations shown in Figure 9, the profiles exhibited here include contributions from the temperature dependence of the unit cell volume as well as that of the solute−polymer energy of interaction, $U(r,\Theta)$.

Overall, for both gases, the present study indicates a strong dependence of k_H with temperature in the glassy regime (low temperatures, large t) as well as the presence of a minimum around the glass transition temperature of the polymer. The study reported by Sato[21] suggests that usually the glass transition temperature for the polymer matrix is also the temperature of minimal solubility for noble gases. This statement is supported by sorption measurements of a series of noble gases in polymethylacrylate and could be explained by the contribution to k_H from the filling of voids in the polymer matrix. For N_2 in polystyrene, Sato[21] determines a comparable result. The overall trend of the temperature dependence of k_H for N_2 in PP and the temperature of minimal solubility predicted in this study are both in very good agreement with the noble gas behavior suggested above. Two competing effects are known characteristics for sorption of gases in polymer matrices:[21] gas condensation, dominant at low temperatures, and solute−solvent mixing, increasingly important at higher temperatures. With CO_2's

TABLE 4: Values of k_H (molecules/cell/kPa) Calculated from the Grand Canonical (GC) and Henry's Constant (HCE) Ensembles[a]

	GC			HCE
PET	k_H	c_∞	b	k_H
$+O_2$				
−Langmuir	2.35×10^{-4}	0.05	0.05	2.9×10^{-4}
−Linear	2.35×10^{-4}	0	0	
$+H_2O$				
−Langmuir	1.16×10^{-4}	0	0.99	1.0×10^{-4}
−Linear	1.16×10^{-4}	0	0	

[a] Equation 4 is used to fit the concentration versus pressure data via a Langmuir (both terms) or linear (first term only) expression. The R^2 values for the fit of the GC ensemble data are 0.96 for oxygen and 1 for water. Equation 8 is used for the HC calculations.

TABLE 5: Henry's Constants ($cm^3\ kg^{-1}\ MPa^{-1}$) for CO_2 and N_2 in PP Measured at 461 K[20] [a]

	k_H (CO_2)	k_H (N_2)
Durrill and Griskey[20]		
461 K	2250 ± 180	1310 ± 110
Sato et al.[21]		
461 K	2830	971
453 K	2729	921
MD simulations (453 K)	$1630 < k_H \leq 2570$)	$737 < k_H \leq 1063$

[a] In the present MD study, the limits for k_H corresponding to a 95% confidence interval are calculated from an MD trajectory at 453.2 K. From Sanchez−Lacombe-type equations,[21] k_H at 461 and 453 K are calculated. The range calculated from the MD simulations includes the experimental value.

TABLE 6: Solubility Constants of Oxygen in PVDC, PP, PET, and PVOH (ordered from Least to Highest Soluble)[a]

polymer	ρ_{exp} g/cm^3	k_H molecules/cell/kPa	k_H cm^3/cm^3/atm
PVOH	1.29	$(5.2 < \mu \leq 6.4) \times 10^{-4}$	$0.41 < \mu \leq 0.50$
PET	1.34	$(6.2 < \mu \leq 9.2) \times 10^{-4}$	$0.46 < \mu \leq 0.68$
PP	0.86	$(1.0 < \mu \leq 1.4) \times 10^{-3}$	$0.53 < \mu \leq 0.74$
PVDC	1.66	$(1.7 < \mu \leq 2.1) \times 10^{-3}$	$0.75 < \mu \leq 0.92$

[a] The interval of variation for k_H is calculated for a 95% confidence level. The solubility values do not follow the experimental[1] trend of oxygen permeabilities (from lowest to highest: PVOH < PVDC < PET < PP) most probably due to the fact that PP and PVDC, being at 300 K in the glassy regime, are diffusion dominated. Experimental oxygen permeabilities range over 4 orders of magnitude; the calculated solubilities only differ by a factor of 2.

TABLE 7: Solubility Constants for Water Vapor in PVOH, PET, PVDC, and PP (Ordered from Least to Highest Soluble)[a]

polymer	ρ_{exp} g/cm^3	k_H molecules/cell/kPa	k_H cm^3/cm^3/atm
PP	0.86	$(2.4 < \mu \leq 4.2) \times 10^{-4}$	$0.13 < \mu < 0.22$
PVDC	1.66	$(1.4 < \mu \leq 2.2) \times 10^{-2}$	$6.5 < \mu < 10.2$
PET	1.34	$(1.3 < \mu \leq 2.9) \times 10^{-1}$	$96 < \mu < 214$
PVOH	1.29	$0.3 < \mu \leq 1.3$	$235 < \mu < 1017$

[a] The interval of variation for k_H is calculated for a 95% confidence level. The solubility values for water vapor follow more closely the experimental[1] trend of permeabilities (from lowest to highest: PVDC < PP < PET < PVOH). Both experimental water vapor permeabilities and calculated solubilities range over 4 orders of magnitude.

critical temperature higher than that of N_2, gas condensation is also more important for the former. Over the same temperature range, k_H values for CO_2 in PP are larger than those of N_2, the difference (2−5 times larger at temperatures below the melting temperature of PP) decreasing with increasing temperature (Figure 8). Our study is the first to account for such interactions

TABLE 8: Average Values of Total Volume, Densities, and Oxygen Solubility Calculated Using HCE for the Minimized Polymer Samples Generated with the CED Procedure[a]

polymer	V_{cell} Å^3	density g/cm^3	k_H molecules/cell/kPa
PVOH	4857 ± 89	1.21 ± 0.02	$(0.1 < \mu \leq 4.9) \times 10^{-4}$
PET	4888 ± 88	1.31 ± 0.02	$(0.1 < \mu \leq 4.8) \times 10^{-4}$
PP	6879 ± 189	0.81 ± 0.02	$(1.6 < \mu \leq 5.8) \times 10^{-4}$
PCTFE	8658 ± 335	1.79 ± 0.07	$(1.0 < \mu \leq 1.9) \times 10^{-3}$
PVDC	8233 ± 116	1.56 ± 0.02	$(1.1 < \mu \leq 2.1) \times 10^{-3}$

[a] No direct correlation can be established between density and k_H.

and to model based on first principles the correct temperature behavior of gas solubility below and above the glass transition temperature.

Temperature influences both the dynamics of the polymer matrix and that of the solute leading to changes in the solute−polymer interactions. To extract each of these effects separately and obtain their influence on the fluctuations of the system, two sets of calculations are performed. First, we considered the dynamics of the polymer matrix at 300 K and calculated k_H for the 300−650 K temperature range (the matrix is maintained at a constant temperature, and only the solute is heated). Second, we included the temperature dependence of the polymer dynamics (both polymer matrix and solute are heated simultaneously). According to eq 7, the first case should lead to values of k_H that scale inversely proportional with temperature and preserve identical time dependence. Figure 9 provides an illustrative example for eq 7 by showing that, by choosing as a reference the dynamical fluctuations of the polymer matrix at a certain temperature (here 300 K), k_H values for the solvent scale inversely proportional with temperature due to the fact that $U(r,\Theta)$ remains practically unachanged (the heated solvent equilibrates rather quickly with the surrounding). Together, Figures 9 and 10 illustrate better how the temporal and temperature dependence of the solute−solvent interactions contribute to the overall temporal and temperature dependence of k_H. Although data for CO_2 are not shown, both N_2 and CO_2 lead to similar behaviors.

According to eq 7, the temperature dependence of k_H shown in Figure 10 is determined by variations in the unit cell volume (V_{cell}) as well as the energy of interaction $U(r,\Theta)$ between the solute and the polymer. Especially at temperatures close and above the melting temperature (T_{melt}) of the polymer, the total unit cell volume exhibits larger fluctuations. The solute−polymer interaction energy, $U(r,\Theta)$, determined by the "chemistry" of the internal surface of the pores, will also change as the polymer chains will have an increased chance to modify their configurations.

4.2. Water and Oxygen Permeabilities. The solubilities of oxygen (Table 6) and water vapor (Table 7) in PET, PVOH, PVDC, and PP at 298 K are calculated using HCE from a 200 ps NPT−MD production run. Each of the polymer samples are generated according to the procedure described in Section 2. The contribution from electrostatic interactions is only included in the solubility calculations for water vapor and not for oxygen.

According to Figure 1, of the four polymeric membranes investigated in the present study, the most oxygen permeable membrane is PP followed by PET, PVDC, and PVOH. The solubilities calculated in the present study predict that PVDC (Tables 6 and 8) is the highest oxygen soluble membrane of the selected four, followed by PP, PET, and PVOH. It should be noted that the oxygen solubilities calculated in the present study for these four polymers differ only by a factor of 2 and the corresponding experimental permeabilities, between the

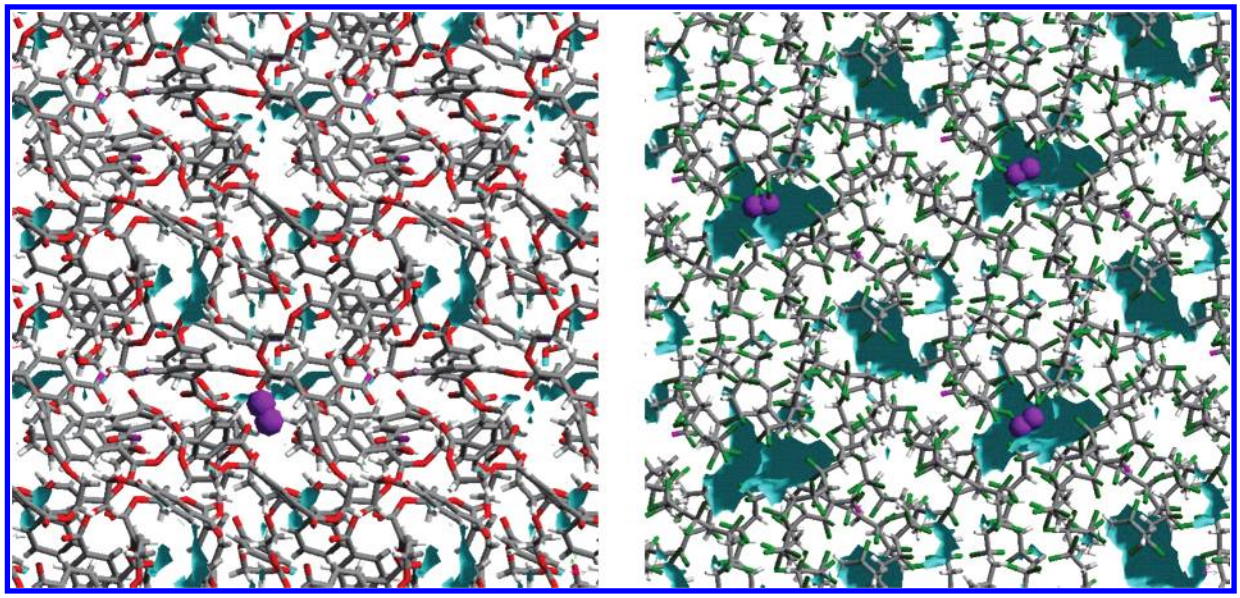

Figure 11. According to the present study, the oxygen solubility of PVDC is twice that of PET and reducing the occupiable volume acts as a mechanism in achieving low solubilities. Two snapshots taken at 100 ps from a molecular dynamics trajectory of PET (left) and PVDC (right) display the oxygen molecules in van der Waals representation (purple) and the distribution of occupiable volume (light blue) as calculated with a probe radius of 1.2 Å.

highest and least permeable, range over 4 orders of magnitude. Figure 11 shows two representative snapshots taken at 100 ps from the molecular dynamics trajectories at 300 K generated for low (PET) respectively high (PVDC) oxygen soluble polymers.

For water, our calculations (Table 7) predict that the most soluble membrane is PVOH followed by PET, PVDC, and PP. Experimentally, PVOH is also the most permeable water membrane, followed by PET, PP, and PVDC. That PVOH has the highest solubility for water is probably explained by the presence of hydrogen bonds between the terminal OH groups (Figure 2) and water molecules. Some hydrogen bonds may also be present in the case of PET between the backbone or side oxygen atoms and water molecules (Figure 2).

When comparing hierarchies of solubilities and permeabilities, temperature is an essential parameter as it determines the glassy (diffusion dominated) or rubbery (solubility controlled) regime of the polymer. For example, of the four polymers for which oxygen and water vapor solubilities are calculated in the present study both PP and PVDC are in the glassy regime and thus are diffusion dominated. Tables 6 and 7 show that, except for PP, the selected polymer membranes are characterized by solubilities larger for water than for oxygen.

The confidence limits of the k_H values in Tables 6−8 are calculated for values determined along an MD trajectory. These large confidence limits are strongly correlated with the k_H temporal fluctuations (Figures 9 and 10). As discussed in Section 4 for nitrogen and carbon dioxide solubility in PP, the thermal fluctuations of the polymer matrix (total volume of the unit cell) during the molecular dynamics run are one important source for such large fluctuations. Figure B2.1 (see Supporting Information) shows such a variation for the PP sample and may be considered representative for the dynamics of all the polymers investigated in the present study. A second cause for the observed temporal fluctuations of k_H is the "chemistry" of the internal surface of the voids that is captured in the solute−polymer interaction energy, $U(r,\Theta)$. The value of $U(r,\Theta)$ is sensitive to modifications in the configurations of the polymer chains. Other mechanisms that may contribute to such large confidence limits are also discussed below.

Factors like polymer crystallinity, tacticity, orientation, conformational properties, and cross-linking certainly influence the permeability properties of the formed membrane.[5,6] For example, polymers characterized by a high degree of crystallinity normally exhibit lower permeabilities. In PTFEP, crystalline domains do not restrict gas diffusivity, but they significantly reduce gas solubility in semicrystalline PTFEP through reduction of amorphous content and additional effects (chain immobilization) of the crystallites on amorphous-phase solubility.[5] Recently it has also been shown experimentally[25] that some clay/polymer composites may offer significantly reduced permeabilities over the individual polymer materials. This can be explained partly by the added tortuosity of the path that a gas molecule or atom must take to transverse the polymeric nanocomposite membrane due to the combination of crystalline and amorphous regions. A study performed on copolymers of styrene and its homopolymer[4] indicate that diffusion coefficients and solubility coefficients follow reverse orders. Matrix mobility is the dominant factor influencing diffusion; solubility coefficients depend on the free volume distribution of the matrices.

On the basis of the total free volume (total volume within a cell not occupied by atoms) and its distribution, one would expect that higher density polymers should in principle exhibit lower solubilities and denser polymers to expand their confidence limits over a smaller range. Also for denser polymers, one would expect the confidence limits to expand over a smaller range. Solubility values and their corresponding confidence limits calculated in the present study do not exhibit such a correlation. For both oxygen and water vapors, k_H values (Table 6−8) are larger for the higher density polymers and confidence intervals are comparable. The modeled polymer samples are, however, of low molecular weight, and thus, the presence of a larger number of terminal ends than characteristic for the real polymer matrix could add an important contribution to the calculated sorption values.

Also, there seems to be no dependency of the k_H confidence intervals with the chemical structure of the investigated polymers. Systems like PP, PVOH, and PVDC that do not contain aromatic rings have higher flexibility and could possibly easily explore a larger number of conformations. Such movements

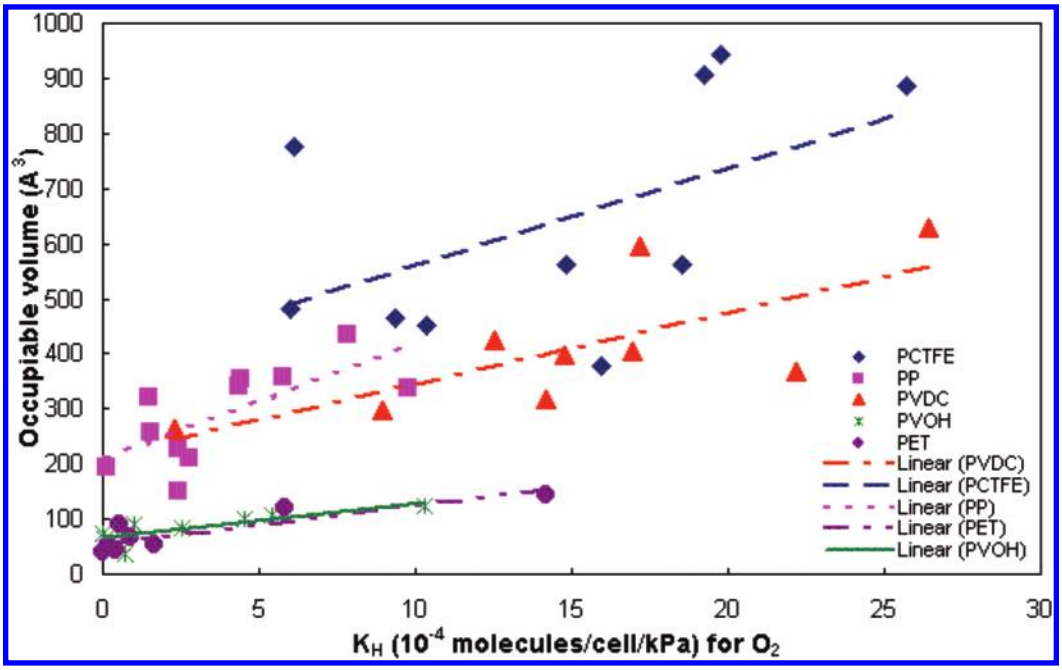

Figure 12. Oxygen sorption vs total occupiable volume of the five polymer matrixes for the energy minimized samples generated via the anneal dynamics (CED) procedure. The probe radius in the calculation of occupiable volume is 1.2 Å. Relatively good correlations are observed for PP, PVDC, and PCTFE but not for PET and PVOH. Additional data show that actually the distribution of free volume within the unit cell is rather more important than the total occupiable volume.

would allow "bad configurations" to be eliminated during the dynamics simulation and reduce the fluctuations in k_H values. The data in Tables 6−8 do not seem to indicate such correlations: the confidence interval for PET is comparable to those of the other polymers.

Terminal ends of the polymer chains could also influence their dynamics and thus, the confidence interval determined for k_H. An infinite molecular weight chain of PET is constructed by building many times the polymer unit cell for finite chains. When terminal groups are located close to each other, they are connected. From 200 ps of MD at 298 K, the solubility of oxygen calculated for this infinite molecular weight PET sample is found to be $(5.8 < \mu \leq 8.0) \times 10^{-4}$ molecules cell^{-1} kPa^{-1}, with a confidence interval for k_H of about 40%, comparable with that in Tables 6 and 8. Also as noted before, the density of the infinite molecular weight chain is accurately reproducing the experimental value for this polymer.

The detailed study of the temperature dependence of the k_H of nitrogen and carbon dioxide performed for the case of polypropylene did not include the range of extreme temperatures (1000 K). A 200 ps MD trajectory is generated at 1000 K for the PET sample. The k_H for oxygen is calculated as $(5.9 < \mu \leq 8.5) \times 10^{-6}$ molecules cell^{-1} kPa^{-1}. Compared to the confidence interval at 298 K, $(6.2 < \mu \leq 9.2) \times 10^{-4}$ molecules cell^{-1} kPa^{-1}, the average value decreased by 2 orders of magnitude but the width of the confidence interval remained comparable (~45%).

Experimental investigations show that, especially for highly soluble and dense gases, the quantity of dissolved gas can be appreciable and usually leads to polymer swelling. Naturally, in such cases, a correlation between k_H and either the total or occupiable volume[26] characteristic for the modeled polymer samples should exist. Henry's constants calculated via HCE are plotted as a function of the total occupiable volume for the five polymer samples. None of the polymers exhibit a clear correlation between k_H and the occupiable volume (data not shown). If the total occupiable volume and k_H are calculated for the minimized samples generated with the CED procedure, PP, PVDC, and PCTFE show good such correlations (Figure 12). For PET and PVOH, probably because of the low occupiable volume calculated for these samples, it is difficult to define such correlations. Figure 11 shows the distribution of the occupiable volume for PET and PVDC as calculated with a probe radius of 1.2 Å. Not only is the total occupiable volume smaller in PET than in PVDC, but it is also more fragmented. PVDC exhibits a smaller number of regions but with larger volumes that can be occupied by the test probe while PET exhibits a large number of very small regions.

TABLE 9: Henry's Constant for Oxygen in PET with "Controlled" Occupiable Volumes, V_{oc}, and Void Distributions for the Same Total Volume of the Unit Cell, $V_{UC} = 1311$ Å^3 [a]

sample	S_C Å^2	V_{oc} Å^3	S_{oc} Å^2	k_H molecules/cell/kPa
no O_2	1367	293	370	5.5×10^{-3}
1×10 O_2	2032	398	507	4.5×10^{-3}
2×5 O_2	1975	472	630	4.5×10^{-3}
10×1 O_2	1745	354	431	2.7×10^{-2}

[a] The surface accessible area of the unit cell, S_C, and the surface area corresponding to the occupiable volume, S_{oc}, are also calculated. The distribution of free volume within the polymer matrix is more important for solubility properties than the total free volume.

An additional test is designed in which PET samples (10 chains with a degree of polymerization of 5) are built (using the Amorphous Builder module of Cerius2)[8] with identical total unit cell volumes ($V_{UC} = 1311$ Å^3) but with controlled void distributions by including during the building procedure (1) no oxygen molecules, (2) one cluster containing ten oxygen molecules, (3) two clusters, each with five oxygen molecules, and (4) ten clusters each containing one oxygen molecule.

Prior to calculating k_H, each of the above samples is minimized and the oxygen molecules removed. The k_H values are summarized in Table 9.

When no oxygen molecules are included in the amorphous building procedure (case 1) the cell will contain the smallest amount of total occupiable volume but include a few large

TABLE 10: Henry's Constant Confidence Intervals for Oxygen in PET for Two Sample Sizes, $n = 10$ and 100, and from Trajectory Averaging[a]

n	k_H (molecules/cell/kPa)
10	$(0.1 < \mu \leq 4.8) \times 10^{-4}$
100	$(4.5 < \mu \leq 6.4) \times 10^{-4}$
trajectory	$(6.2 < \mu \leq 9.2) \times 10^{-4}$

[a] For larger sets of polymer samples, the ensemble average becomes representative of the trajectory average.

volume regions, which could explain why k_H is not the lowest from the four cases. This value is about 1 order of magnitude larger than the trajectory determined value ($6.2 \times 10^{-4} < \mu \leq 9.2 \times 10^{-4}$ molecules/cell/kPa) probably because during MD the void space is redistributed. Between the case of a single large void (case 2, $k_H = 4.5 \times 10^{-3}$ molecules/cell/kPa) and ten small isolated voids (case 4, $k_H = 2.7 \times 10^{-2}$ molecules/cell/kPa), the total occupiable volume (and the corresponding surface area) is decreased by 11% and k_H increases by a factor of 6. Between one void with ten oxygen molecules (case 2) and two voids each containing five oxygen molecules, the total occupiable volume is increased by ~19% but the k_H values are similar.

This test indicates, in agreement with the study by Kucukpinar,[4] that not the total occupiable volume but the distribution of the free volume within the polymer matrix is relevant for solubility calculations. If several small regions that may still accommodate the solute molecule make up the total occupiable volume, then k_H will be larger than for the case when few large voids and many very small ones define it.

To test if it would be more rigorous to use ensemble averages rather than trajectory (time) averages, k_H confidence levels are calculated for the minimized samples ($n = 10$) generated with the CED procedure (Table 10). The results show that the confidence intervals determined as ensemble averages are much larger than those obtained from average trajectory calculations (Tables 6−7). The confidence interval determined from the larger set of polymer samples ($n = 100$) is reduced by 50% compared to that determined from the smaller set. The three calculated confidence intervals differ significantly although some overlap is observed. As an alternative method, accurate solubility values could be determined by performing k_H calculations on a large sample set ($n > 100$) generated with the CED procedure.

During MD, a certain region of the phase space is explored; thus, favorable and unfavorable polymer conformations—defined from the point of view of the interactions with the solute—are sampled. To study the effect of such conformational changes on k_H, frames are extracted from the PET MD trajectory at 298 K corresponding to $V_{av} = 4882.2 \pm 74.9$ Å^3, $V_{min} = 4724.3$ Å^3, and $V_{max} = 5182.1$ Å^3 volumes. Such snapshots capture different configurations of the polymer matrix. The corresponding oxygen solubilities (Table 11a) differ by 3 orders of magnitude with the largest value (3.1×10^{-4} molecules/cell/kPa) corresponding to V_{max}, which also has the largest occupiable volume, and the smallest value (1.7×10^{-7} molecules/cell/kPa) calculated for V_{min} with the smallest occupiable volume.

To maintain the same polymer configurations, the frame at $t = 0$ is successively scaled (using fractional coordinates) to the average, minimum, and maximum volumes extracted from the MD trajectory (Table 11b). This scaling also preserves the distribution of voids and only changes the total occupiable volume. There is a much smaller spread (factor of 6) between oxygen solubility data corresponding to the scaled CED structures. This range directly correlates to the distribution of the occupiable volume.

Additional energy minimization of the CED scaled structures (Table 11c) leaves the V_{max} structure and corresponding k_H practically unchanged. The total occupiable volume of the average and minimum volume structures is smaller by 17% and 32%, respectively. The k_H values are also smaller by 77% and 95%, respectively, the value corresponding to the minimum volume structure becoming smaller than that for the average volume structure. During energy minimization, the polymer structure is relaxed and leads to decreased occupiable volume without it being redistributed. This is a situation where a reduction in solubility (Table 11) directly correlates to a reduction in the total occupiable volume. The unit cell reaches its maximum volume after 2 ps. In such a short MD interval, the polymer configuration did not have time to change significantly, and consequently, the occupiable volume did not redistribute. This could explain why the three values of k_H in Table 11 corresponding to the maximum unit cell volume from the MD snapshot, scaled CED structure, and scaled CED structure with additional minimization are identical. Consequently, the three values of k_H in Table 11 corresponding to the maximum unit cell volume from the MD snapshot, scaled CED structure, and scaled CED structure with additional minimization are identical.

The CED procedure used to generate the polymeric samples from the present study was designed with the purpose of providing a fast and reliable way to generate equilibrated structures. This is much more effective than simple brute MD. To prove this point, we performed the following procedure and we summarized the CED (cal/cc) values in Table 12.

(1) For four polymers (PET, PP, PVDC, PVOH), using the standard CED procedure described in Section 2, which uses only short (10 ps) equilibration times, we took the lowest and highest cohesive energy density samples and ran an additional 1 ns of MD on each. CED values from this 1 ns MD trajectory were compared for the 100−200 ps and 500 ps to 1 ns segments.

(2) Additionally, for the most complex polymer (PET), on the basis of the size of its monomer, we also built samples using the amorphous build procedure, a short minimization and quenching followed by 1 ns of molecular dynamics.

For PVOH and PVDC, the CED values calculated from 200 ps and 1 ns of MD are comparable and also independent if the initial structure corresponds to the lowest or highest energy CED sample generated in the CED procedure. For PP, the CED values from 200 ps are comparable within uncertainties with the values calculated from 1 ns but, overall, higher than the initial CED values of the sample. For PET, which is the most complex and also rigid structure of the polymer samples selected for the present study, the CED values from 200 ps and 1 ns are comparable within uncertainties, independent of the starting structure (low or high CED, small ($n = 10$) or large ($n = 100$) generated set).

For most of these systems, the addition of kinetic energy during the 200 ps−1 ns MD run has acted in decreasing their cohesive energy density proving that longer dynamics may not necessarily lead to better equilibrated samples.

A sample generated using the amorphous builder module of Cerius2[8] and not annealed with the CED procedure but subject to a long (1 ns) brute MD run results in a poorly equilibrated structure (CED values approximately 1 order of magnitude less negative).

Together with the discussion of Section 2 on the statistical adequacy of the CED procedure, these results show that, to achieve good CED values, it is more important to have well

TABLE 11: Henry's Constant, k_H, for Oxygen in PET for Frames Selected from MD Trajectory with Average (4882.2 ± 74.9 Å^3), Minimum (4724.2 Å^3), and Maximum (5182.2 Å^3) Volumes or Scaled (using Fractional Coordinates) from the Initial Frame at $t = 0$ to Have Volumes Equivalent to Average, Minimum, and Maximum[a]

frame	V Å^3	V_{occ} Å^3	k_H molecules/cell/kPa	observations
MD	4882.2	43.1	6.3×10^{-6}	frame at 190 ps, V_{av}
	4729.2	23.9	1.7×10^{-6}	frame at129 ps, V_{min}
	5187.5	130.6	3.1×10^{-4}	frame at 2 ps, V_{max}
CED	4882.2	79.9	3.4×10^{-4}	$t = 0$, scaled to V_{av}
	4724.6	68.0	3.7×10^{-4}	$t = 0$, scaled to V_{min}
	5182.2	110.4	3.1×10^{-4}	$t = 0$, scaled to V_{max}
CED	4882.2	65.9	7.6×10^{-5}	t = 0, scaled to V_{av} and minimized
	4724.6	47.2	1.6×10^{-5}	$t = 0$, scaled to V_{min} and minimized
	5182.2	118.1	3.1×10^{-4}	$t = 0$, scaled to V_{max} and minimized

[a] Scaling the volume of the polymer ensures that the polymer conformation and free volume distribution remains unchanged and allows us to study the correlation between solubility and occupiable volume. For similar values of the occupiable volume and different polymer conformations (CED versus MD), solubilities may change as much as one order of magnitude.

TABLE 12: Comparison of Standard CED Results[a] with a Procedure Using Long Molecular Dynamics Runs Alone[b]

polymer sample		cohesive energy densities (CED) (cal/cc) initial (CED)	average 500 ps−1 ns	100−200 ps
PET				
10-sample set	average	−142.6 ± 10.7		
	high	−125.9	−198.3 ± 21.6	−171.2 ± 15.1
	low	−155.0	−201.8 ± 11.9	−201.9 ± 21.0
100-sample set	average	−151.5 ± 11.4		
	high	−127.3	−217.7 ± 29.3	−179.3 ± 12.7
	low	−176.68	−184.7 ± 19.4	−183.4 ± 17.1
amorphous build		28.6	−18.3 ± 11.8	−14.6 ± 7.6
PP				
10-sample set	average	−48.0 ± 5.0		
	high	−43.2	−31.4 ± 26.9	−20.5 ± 18.8
	low	−53.2	−33.8 ± 22.7	−41.4 ± 20.8
PVDC				
10-sample set	average	−60.6 ± 2.6		
	high	−56.5	−72.3 ± 6.4	−74.4 ± 7.9
	low	−64.2	−71.8 ± 5.2	−71.2 ± 6.8
PVOH				
10-sample set	average	−262.7 ± 16.4		
	high	−232.9	−242.4 ± 26.5	−230.9 ± 17.5
	low	−287.7	−253.7 ± 23.1	−232.2 ± 11.0

[a] This work. [b] More negative means better packed and more favorable cohesive energy densities. Without the CED procedure (see amorphous build line for PET), the cohesive energy densities are, in absolute value, too low.

prepared samples (as developed in the CED procedure) than to perform long (∼nanoseconds) brute force molecular dynamics. Consistent with this, we note (Table 3) that the lowest energy CED generated samples lead to polymer densities in closest agreement to experimental densities, with deviation of CED densities from experimental values of less than 4%. We surmise that long MD runs are not likely to find good equilibrated structures for amorphous polymers so that the reliability and accuracy of CED is best determined by comparing the CED procedure results directly with experimental data (despite the issue of relying on the FF).

The invariance of the values and confidence limits determined for k_H with respect to the length of the MD production run again indicate that longer simulation times would give more accurate determinations for complex structures such as PET; for more flexible (faster equilibrating) samples, the confidence intervals remain unchanged.

5. Conclusions

The present study describes a combined molecular dynamics and Monte Carlo methodology to estimate solubility properties of polymeric membranes (PP, PET, PVDC, PVOH) with respect to a variety of solutes (nitrogen, carbon dioxide, oxygen, and water).

We thoroughly describe the generation of these polymer samples via an amorphous builder procedure, which uses information contained in rotational isomeric state tables individually calculated for each polymer followed by an annealing cycle (the cohesive energy density procedure). We present a detailed analysis of the cohesive energy density (CED), binding energy (E_b), and strain energy (E_s) for two sets of samples ($n = 10$ and 100) generated for the PET polymer. Ideally, the larger the sample set, the more accurate the calculated properties and the better configurations with lower energies will be represented. Boltzmann averages and probability distributions of CED, E_b, and E_s indicate that configurations in the smaller set are biased toward configurations with higher CED and E_b energies due to larger existing strain energy within the unit cell. However, the lowest CED energy sample from the smaller set is representative for the average structure of the larger set and provides a reliable criterion for sample selection. To obtain well equilibrated samples with good CED values, it is desired to have well prepared samples rather than performing long (∼nanoseconds) brute molecular dynamics. Performing 200 ps of MD on samples generated using the CED procedure (low, average, or high CED) results in comparable (within uncertainties) trajectory average CED values. Performing 1 ns of MD on samples constructed using the amorphous build results in 1 order of magnitude less

cohesive structures then when equilibrated using the CED procedure. The CED procedure employed in the present study provides a fast, reliable, and accurate method to generate well equilibrated samples with careful consideration given to more complex and rigid structures.

Infinite rather than low molecular weight samples should preferably be constructed to best match experimental densities. For the present study, however, such samples would increase the computational time for solubility calculations beyond the intended purpose.

Despite the fact that in the present study samples of amorphous polymers with low molecular weights are constructed and short molecular dynamics runs (200 ps) are used to calculate solubility coefficients, the employed HCE method provides a useful and relatively quick tool to better understand the process of gas solubility in polymeric matrixes.

For noble gases, the correct trend of solubilities with temperature, below and above the polymer's melting point, are predicted. We distinctively indicate two contributions to the temperature dependence of the solubility coefficients: one originating from the temperature dependence of the polymer matrix and the other from the temperature dependence of the polymer−solute interactions. The temperature of minimal solubility for N_2 and CO_2 is accurately determined and falls close to the glass transition temperature of the polymer. Additional validation of several properties of the polymer matrix (compressibility, thermal expansion coefficient) is provided. The influence of the values for the mass cell prefactor (MCPF) coefficient on the volume fluctuations of the polymer and on the determined solubility values is also discussed (See Supporting Information).

Our calculations indicate that the polymeric membranes selected in the present study (PP, PET, PVOH, PVDC) are characterized by larger water than oxygen solubilities, especially in polymer matrices where hydrogen bonding and electrostatic interactions prevail.

For statistical accuracy, a confidence interval rather than an average value is calculated for k_H. They are also a result of a series of factors, each separately investigated in our study: sample equilibration and dynamics, total occupiable volume, size of voids and their distribution, and interaction energies of the solute−polymer matrix determined by "favorable" or "nonfavorable" exposed polymer chains. Our conclusion is that the large confidence intervals determined for the gas solubility values have to be regarded as a characteristic of each polymer, directly related to its structural properties and the nature of its interactions with the solute.

What makes a polymeric membrane a good barrier? The answer is a combination of low solubility and low diffusion coefficients. We summarize below possible ways to achieve such a combination based on the results of the present study and of a similar analysis performed for diffusion coefficients.[27]

Low diffusion coefficients in general are achieved by increasing the tortuosity of the path of a gas molecule and also by reducing the amount of accessible volume. This has been accomplished for example with multilayered materials or clay nanocomposites. Flat, long particles create impenetrable surfaces and introduce additional pathways that require additional time for the gas molecules to overcome. A low solubility environment will also not lead to steady state and will promote a transient process based on tortuosity. Alternative solutions for increasing the topological difficulty of the landscape for diffusion include the use of tackifiers, polymers characterized by high glass temperatures, cross-linked polymers, or copolymers.

Low solubility may be achieved by making molecules "unhappy" and reducing the number of "felicitons" within the structure. Typically, "feliciton" regions are characterized by high compressibility values (such as those found near chain ends or side chains) or places where electrostatic interactions (for the case of polar molecules, such as water) or van der Waals interactions (such as in the case of oxygen) occur. In general, high densities correlated with low free volume and high cohesive energies of the polymers will limit the solubility of nonpolar molecules. For polar molecules, an additional concern is related to the presence of polar groups, which provides again a favorable interaction environment. In general, a polymer with a high contact angle such as fluorinated polymers will provide a good barrier for water where solubility is concerned. Reducing the mobility of the polymer matrix as well as the distribution of the free (occupiable) volume would act as mechanisms toward lowering both the gas solubility and the diffusion coefficients.

Acknowledgment. We would like to thank Alejandro Strachan for his contribution and valuable suggestions in the initial stages of this project. We thank R. Niemer and Y. Zhou with help in building some of the polymer samples used in this study. This work was supported in part by a grant from the Avery Dennison Corporation. The facilities of the MSC are partly funded by NSF, DOE-ASCI, Chevron, NIH, ONR, Seiko-Epson, Kellogg's, General Motors, Beckman Institute, Asahi Chemical, and Nippon Steel.

Supporting Information Available: Summary of the rotational isomeric state tables and the charges on the five polymer samples (PET, PP, PCTFE, PVDC, and PVOH), compressibility and thermal expansion coefficients, mass cell prefactor coefficient, and related figures.

References and Notes

(1) *Permeability and other film properties of plastic and elastomers*; Plastic Design Library: Norwich, NY, 1995.

(2) A similar expression of permeability can be derived for the permeant being a liquid.

(3) Neyertz, S.; Douanne, A.; Brown, D. *Macromolecules.* **2005**, *38*, 10286.

(4) Kucukpinar, E. and Doruker, P. *Polymer* **2003**, *44*, 3607.

(5) Hu, N. and Fried, J. R. *Polymer* **2005**, *46*, 4330.

(6) Economou, I. G. *Fluid Phase Equilib.* **2005**, *228*, 15.

(7) Kashilara, S.; Iotov, M.; Dasgupta, S.; Gao, G.; Belmares, M.; Goddard, W. A. Unpublished data.

(8) *Cerius2 MSI manual*, Accelrys: San Diego, CA, April 1997.

(9) As for PET, the number of atoms in the polymeric chain is larger than that of the other polymers; a 5-mer instead of a 20-mer, having the same number of atoms as the 20-mers of PP, PCTFE, PVDC, and PVOH was constructed. Due to the presence of chiral centers, for PP and PCTFE, syndiotactic samples were built.

(10) Mayo, S. L.; Olafson, B. D.; Goddard, W. A. *J. Phys. Chem.* **1990**, *94*, 8897.

(11) Hildebrand, J. H. *The Solubility of Non-Electrolytes*, Reinhold Publications Corporation: New York, 1936.

(12) Blanco, M. *J. Comput. Chem.* **2004**, *25*, 1814.

(13) *Polymer Handbook*, 4th ed.; Brandrup, J., Immergut, E. H., Grulke, E. A., Eds.; John Wiley & Sons Inc.: New York, 1999.

(14) Muller-Plathe, F. *Macromolecules* **1991**, *24*, 6475.

(15) Stanett, V. T. *Adv. Polym. Sci.* **1978**, *32*, 69.

(16) Vasile, C. *Handbook of polyolefins*; Marcel Dekker: New York, 2000.

(17) Metropolis, N.; Rosenbluth, A. W.; Rosenbluth, M. N.; Teller, A. N.; Teller, E. *J. Chem. Phys.* **1953**, *21*, 1087.

(18) Allen, M. P.; Tildesley, D. J. *Computer simulation of liquids*, Clarendon Press: Oxford, U.K., 1987.

(19) Bezus, A. G.; Kiselev, A.V.; Lppatkin, A.A.; Pham Quang, Du, *J. Chem. Soc., Faraday Trans.* **1978**, *2*, 74−367.

(20) Durill, P. L.; Griskey, R. G. *AIChE J.* **1996**, *12*, 1147.
(21) Sato, Y. *Fluid Phase Equilib*, **1999**, *162*, 261.
(22) Stern, S. A.; Mullhaupt, J. T.; Gareis, P. J. *AIChE J.* **1969**, *15*, 64.
(23) Reid, R.C. *The properties of gases and liquids*, 4th ed.; McGraw-Hill: New York, 1987.
(24) http://www.diffusion-polymers.com/Gas%20Diffusion.htm.
(25) Vaia, R. A.; Giannelis, E. P. *MRS Bulletin*, May 2001.
(26) The occupiable volume is the fraction of the total volume of the unit cell that can be occupied by a probe of radius R_p (includes isolated voids in the polymer matrix). A probe radius of 1.2 Å was used in the present study.
(27) Strachan, A.; Cozmuta, I.; Blanco, M.; Goddard, W. A. *Multi-scale, hierarchical modeling of membrane barrier properties, Technical Report*; Avery Dennison: August 2001.
(28) Barton, A. F. M. *CRC handbook of polymer-liquid interaction parameters and solubility parameters*; CRC Press: New York, 1990.
(29) Supaphol, P.; Spuiell, J. E.; Lin, J. S. *Polym. Int.* **2000**, *49*, 1473.